ADVANCED MATERIALS
www.advmat.de

Highly Efficient Photosensitizers with Far-Red/Near-Infrared Aggregation-Induced Emission for In Vitro and In Vivo Cancer Theranostics

Dong Wang, Michelle M. S. Lee, Guogang Shan, Ryan T. K. Kwok, Jacky W. Y. Lam, Huifang Su,* Yuchen Cai,* and Ben Zhong Tang**

Fluorescence-imaging-guided photodynamic therapy has emerged as a promising protocol for cancer theranostics. However, facile preparation of such a theranostic material for simultaneously achieving bright emission with long wavelength, high-performance reactive oxygen species (ROS) generation, and good targeting-specificity of cancer cells, is highly desirable but remains challenging. In this study, a novel type of far-red/near-infrared-emissive fluorescent molecules with aggregation-induced emission (AIE) characteristics is synthesized through a few steps reaction. These AIE luminogens (AIEgens) possess simple structures, excellent photostabilities, large Stokes shifts, bright emission, and good biocompatibilities. Meanwhile, their ROS generation is extremely efficient with up to 90.7% of ROS quantum yield, which is far superior to that of some popularly used photosensitizers. Importantly, these AIEgens are able to selectively target and ablate cancer cells over normal cells without the aid of any extra targeting ligands. Rather than using laser light, one of the presented AIEgens (MeTTPy) shows a remarkable tumor-targeting photodynamic therapeutic effect by using an ultralow-power lamp light (18 mW cm^{-2}). This study thus not only extends the applications scope of AIEgens, but also offers useful insights into designing a new generation of cancer theranostics.

In view of the fact that cancer is increasingly a global health issue, developing effective technologies for cancer diagnosis and therapy remains an urgently needed and challenging task facing scientists. Among numerous advances that have been made, cancer theranostics that allow the ingenious integration of accurate diagnosis with targeted therapeutics in a single formulation within spatial colocalization, have aroused increasing attention in both research and clinical fields,[1–3] because the utilization of theranostics is promising to achieve the maximization of therapeutic efficacy, the optimization of drug safety, the improvement of pharmacokinetics, as well as assisting in streamlining the drug development process.[4,5] Although a large number of theranostic systems have been exploited and used in cancer treatment, current situation is still far from ideal. Previously developed theranostic systems have their respective and collective drawbacks including complicated fabrication, unsatisfied diagnosis imaging quality, low therapeutic efficiency, high preparation cost, and cumbersome construction.[6–9] Evidently, the exploration of a facile and straightforward synthetic route to theranostic agents sharing efficient diagnosis imaging, high therapeutic efficacy, and outstanding specificity for cancer treatment and diagnosis is still highly desirable.

Dr. D. Wang, Prof. B. Z. Tang
Center for AIE Research
College of Materials Science and Engineering
Shenzhen University
Shenzhen 518060, China
E-mail: wangd@szu.edu.cn; tangbenz@ust.hk

Dr. D. Wang, M. M. S. Lee, Dr. G. Shan, Dr. R. T. Kwok, Dr. J. W. Y. Lam, Prof. B. Z. Tang
Hong Kong Branch of Chinese National Engineering Research Center for Tissue Restoration and Reconstruction
Department of Chemistry
Institute of Molecular Functional Materials
State Key Laboratory of Neuroscience
Division of Biomedical Engineering and Division of Life Science
The Hong Kong University of Science and Technology
Clear Water Bay, Kowloon, Hong Kong 999077, China

Dr. H. Su
Department of Orthopaedic Surgery
The First Affiliated Hospital of Zhengzhou University
Zhengzhou University
Zhengzhou 450052, P. R. China
E-mail: suhuif@mail2.sysu.edu.cn

Dr. Y. Cai
State Key Laboratory of Oncology in South China
Collaborative Innovation Center for Cancer Medicine
Sun Yat-sen University Cancer Center
Guangzhou 510060, China
E-mail: caiych@sysucc.org.cn

The ORCID identification number(s) for the author(s) of this article can be found under https://doi.org/10.1002/adma.201802105.

DOI: 10.1002/adma.201802105

Among diverse diagnosis imaging techniques, fluorescence imaging (FLI) has been recognized to be a noninvasive and powerful tool for cancer diagnosis by virtue of its low cost, superb sensitivity, excellent temporal resolution, and good reproducibility.[10,11] In addition, as a minimally invasive and reliable cancer-therapy modality with high spatiotemporal precision, photodynamic therapy (PDT) that is driven by activating photosensitizer (PS) to generate cytotoxic reactive oxygen species (ROS) to induce cell death upon light irradiation, has been gaining increasing attention from both researchers and physicians.[12–16] Compared to chemotherapy, the use of PDT can avoid cell resistance toward drugs, and display minimized side effects, thanks to its light controllable feature.[17] Taking the intrinsic advantages of both FLI and PDT, FLI-guided PDT has emerged as a promising alternative for cancer treatment.[18–20] An ideal PS for FLI-guided PDT must possess several inherent characteristics such as high fluorescence brightness, relatively long wavelengths of absorption and emission, highly efficient ROS generation, outstanding photostability, and good biocompatibility.[21,22] However, conventional PSs usually suffer from some defects, such as inefficient fluorescence emission in aggregation state resulting from aggregation-caused quenching (ACQ) phenomenon, insufficient ROS production, and lacking of combination capability of efficient emission with sufficient ROS production. In a related context, the emergence of PSs with aggregation-induced emission (AIE) characteristics could perfectly address these issues. As an anti-ACQ phenomenon, AIE was established in 2001 by Tang's group,[23] which refers to a unique phenomenon that some propeller-shaped fluorophores are nonemissive or weakly emissive in the molecularly dissolved state but they emit intensively in aggregated states through a mechanism of the restriction of intramolecular motions (RIM).[24,25] The AIE properties endow AIE luminogens (AIEgens) with attractive characteristics in FLI, including high emission brightness in aggregates, high photobleaching threshold, great tolerance for any concentrations, large Stokes shift, and great potential as "light-up" probes.[7,26–28] Moreover, it has been demonstrated that AIEgens can also provide efficient ROS generation in aggregation state, probably resulting from both: (1) promoted energy transfer from the lowest excited singlet state (S1) to the lowest triplet state (T1) caused by the prohibition of energy dissipation through nonradiative channels,[29] and (2) the mechanism termed "aggregation-induced intersystem crossing" (AI-ISC).[30]

Although the exploration of AIEgens in FLI-guided PDT for cancer theranostics has achieved initial success in past few years, some major problems have yet to be solved.[31,32] For instance, the majority of these AIEgens has short wavelengths of absorption and emission, therefore, aiming to the practical application of in vivo cancer theranostics, synthesis of AIEgens with intense emission in far-red/near-infrared (FR/NIR) region (>650 nm) exhibiting deep penetration, minimal photodamage, and high signal-to-noise (S/N) ratio of imaging is still required.[33,34] The efficiency of ROS generation remains to be enhanced, especially for the development of heavy-atom-free PSs with highly efficient ROS production.[35,36] Additionally, facile construction of cancer cell-specific targeting system with low cost is significantly important but rarely reported.

In this contribution, we develop a simple synthetic strategy involving a few steps reaction to obtain a novel type of AIEgens having intense FR/NIR emissions. These AIEgens possess extremely high ROS generation efficiency, and can inherently target with cancer cells over normal cells without the aid of any extra targeting ligands. The ingenious combination of all the desired features into a single molecular probe makes it ideal for cancer theranostics. Both in vitro and in vivo evaluation showed that these developed AIEgens were effective in cancer theranostics.

The integration of strong electron donor–acceptor (D–A) interaction with extended π-conjugation in the structure of fluorophore could facilitate intramolecular charge transfer (ICT), therefore leading to smaller electronic bandgaps, and longer wavelengths of absorption and emission. In this work, the designed compounds TTPy and MeTTPy (**Figure 1**A) are comprised by pyridinium moiety (working as A), carbon–carbon double bond (π-bridge), thiophene fragment (D and π-bridge), triphenylamine segment (D), and/or two methyl groups (D), indicating extremely high D–A strength. Sufficient rotations of freely rotated moieties of these two compounds could consume the exciton energy upon photoexcitation, resulting in nonemission or weak emission in solution. On the other hand, twisted conformation of triphenylamine segment could enlarge the intermolecular distance, as a consequence, their emission quenching in aggregation state could be prevented due to remarkably reduced intermolecular π–π interaction.[25] The above-mentioned features would enable TTPy and MeTTPy to be AIE-active with long emission wavelengths. Interestingly, enhancement of D–A strength is also one of the key protocols to promote ROS generation efficacy of PSs, because high D–A strength favors separation of highest occupied molecular orbital (HOMO) and lowest unoccupied molecular orbital (LUMO) distribution and ISC process from S1 to T1. It is believed that ISC can also be elevated by the existence of heteroatom components.[37] Therefore, these two compounds potentially having AIE features, strong D–A strength, and heteroatoms (S and N) could be excellent PSs for ROS generation. Furthermore, the pyridinium moiety with positive charge does not only play a role as electron-accepting unit, but also make these two compounds promising for both mitochondria-specific targeting and selective accumulation in cancer cells.[38–40]

To verify these hypotheses, we started with the synthesis. As depicted in Figure 1A, both TTPy and MeTTPy were simply obtained through a few steps reaction. In the primary step, Suzuki–Miyaura coupling reaction was smoothly conducted by employing (5-formylthiophen-2-yl)boronic acid and 4-bromo-N,N-diphenylaniline or its derivative containing methyl groups as starting materials in the presence of palladium catalyst, giving intermediate products **1** in excellent yields. Condensation reaction of presynthesized 1,4-dimethylpyridin-1-ium iodide with **1** then proceeded to produce desired compounds TTPy and MeTTPy with the yields of 86.4 and 83.7%, respectively.

The optical properties of TTPy and MeTTPy were investigated by UV–vis and PL spectroscopies, and summarized in Table S1 (Supporting Information). Their absorption maxima in dimethyl sulfoxide (DMSO) were peaked at 478 and 498 nm, respectively (Figure 1B). The longer absorption wavelength of MeTTPy is ascribed to its smaller HOMO–LOMO energy gap

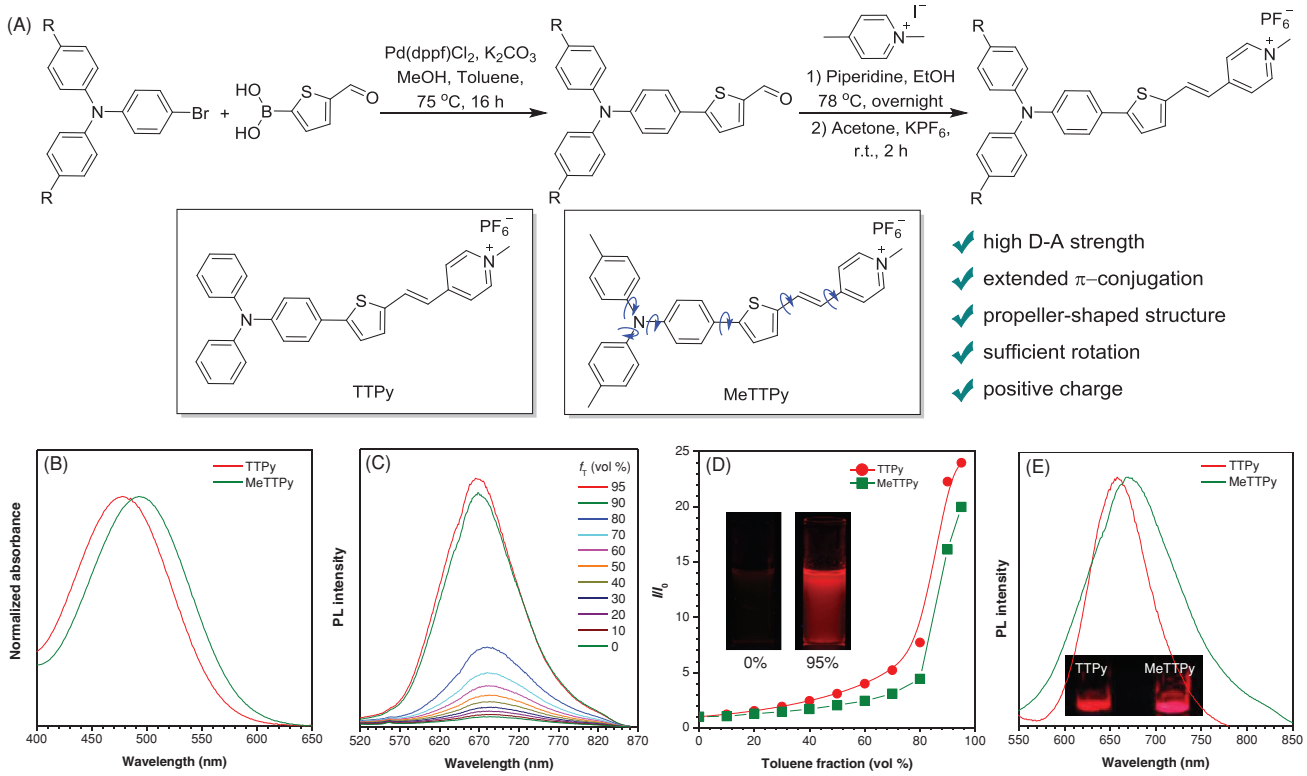

Figure 1. A) Design rationale and synthetic route to TTPy and MeTTPy. B) Normalized absorption spectra of TTPy and MeTTPy in the DMSO solution. C) PL spectra of TTPy (10×10^{-6} M) in DMSO/toluene mixtures with different toluene fractions (f_T); λ_{ex}: 478 nm. D) The plot of the relative emission intensity (I/I_0) versus the composition of the solvent mixture. Inset: Fluorescence photographs of TTPy in the dilute DMSO solution and in DMSO/toluene mixtures with 95% toluene fractions taken under 365 nm UV irradiation. E) Normalized PL spectra of TTPy and MeTTPy in the solid state. Inset: Fluorescence photographs of TTPy and MeTTPy in the solid state taken under 365 nm UV irradiation.

than TTPy (Figure S1, Supporting Information), resulting from the stronger D–A interaction of the emitting center of MeTTPy due to the existence of methyl groups. Density functional theory (DFT) calculations revealed that the electron clouds of the HOMOs are mainly delocalized throughout the whole molecule suggesting good π-conjugation, while both thiophene and pyridinium moieties dominating the LUMO.

DMSO/toluene mixture with different toluene fractions was utilized to assess the AIE properties of TTPy and MeTTPy. Both TTPy and MeTTPy solutions exhibited very weak emissions showing maximal intensities locating at 682 and 687 nm, with 0.5 and 0.3% of quantum yields, respectively. The weak emissions were mainly caused by energy consumption of the excited state through nonradiative pathways owing to the strong molecular rotations in solution state. As revealed in Figure 1C,D, with increasing the fraction of toluene in the solution mixture, the emissions gradually intensified, resulting from the restriction of rotational motions following by the formation of aggregates. Dynamic light scattering (DLS) analysis measurements confirmed the nanoaggregates formation, and the average hydrodynamic diameters of these nanoaggregates that formed in the suspension containing 95% fraction of toluene were determined to be 153 and 137 nm for TTPy and MeTTPy, respectively (Figure S2, Supporting Information). The aggregates of TTPy and MeTTPy were intensely emissive with maxima at 665 and 669 nm, and the emission intensities were boosted with 24- and 20-fold enhancement, respectively (Figure 1D), definitely demonstrating FR/NIR-emissive AIE characteristics. Compared to the solution state, the blueshifted emissions in aggregates can be attributed to the decreased polarity of the local environment upon aggregation formation. In solid state, these two AIEgens emit efficiently in FR/NIR region, and the PL spectra were peaked at 668 and 674 nm, exhibiting relatively high quantum yields of 9.6 and 8.6%, as well as 2.42 and 1.61 ns of lifetime, respectively (Figure S3, Supporting Information). In addition, the emission property of TTPy in different solvents with varied polarities was investigated. As shown in Figure S4 (Supporting Information), upon increasing the solvent polarity from ethyl acetate to acetonitrile, the corresponding emission maximum redshifted from 664 to 691 nm with gradually decreased emission intensity, indicating a typical twisted intramolecular charge transfer (TICT) feature.[41,42]

In the preliminary biological study, cell imaging experiment was conducted. HeLa cells were incubated with 200×10^{-9} M of TTPy or MeTTPy for 30 min, as illustrated in **Figure 2**A–H and Figure S5 (Supporting Information), the reticulum-like mitochondria can be clearly visualized with excellent image contrast to the cell background. Aiming to further evaluate the specificity of these AIEgens to mitochondria, colocalization experiment was performed by costaining with MitoTracker Green, which is a commercially available

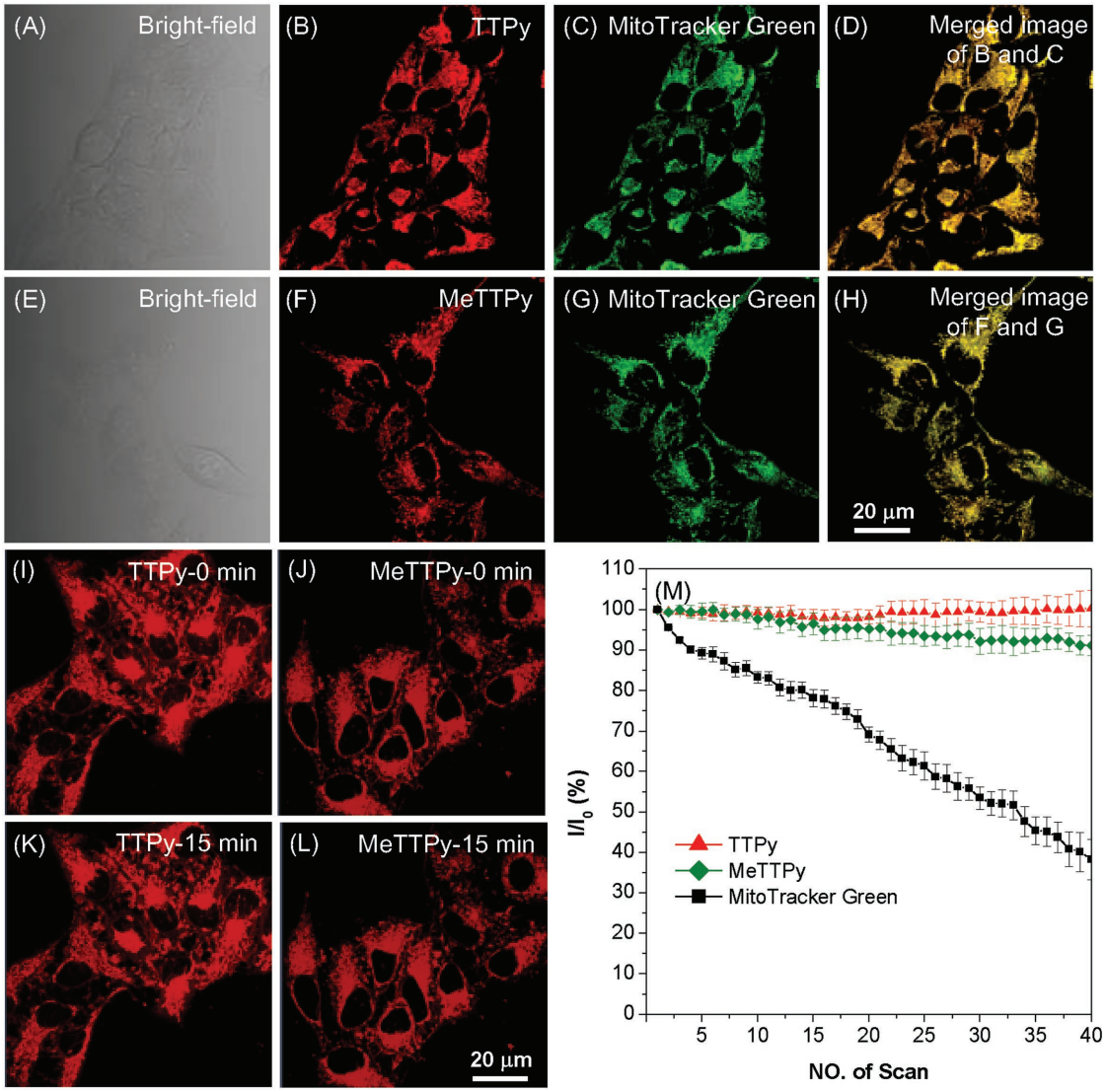

Figure 2. Colocalization test and photostability of AIEgens. A,E) Bright-field, and B,C,F,G) confocal images of HeLa cells stained with (B) TTPy, (F) MeTTPy, and (C, G) MitoTracker Green. D,H) Merged images of (B) and (C), as well as (F) and (G). λ_{ex}: 488 nm (1% laser power). Concentrations: TTPy (200×10^{-9} M), MeTTPy (200×10^{-9} M), and MitoTracker Green (50×10^{-9} M). The emission filter TTPy: 620–744 nm; the emission filter of MitoTracker Green: 490–590 nm. I–K) Confocal images of HeLa cells before (0 min, upper panels) (I,J) and after (K,L) the laser irradiation for 15 min (lower panels) stained with TTPy (I,K) or MeTTPy (J,L). M) Loss in fluorescence of HeLa cells stained with AIEgens and MitoTracker Green with increasing the number of scans of laser irradiation. Concentration: 200×10^{-9} M (TTPy, MeTTPy) and 50×10^{-9} M (MitoTracker Green); λ_{ex}: 488 nm; scanning rate: 22.4 s frame^{-1}; scale bar = 20 μm.

bioprobe for mitochondria. It was demonstrated that the cell imaging of AIEgens and MitoTracker Green perfectly overlapped, and the Pearson's correlation coefficients were 96 and 94% for TTPy and MeTTPy, respectively (Figure S6, Supporting Information), evidently indicating their high specificity for mitochondria-staining. It seems reasonable to infer that their mitochondria-staining behavior could be attributed to the electrophoretic transmembrane migration and upconcentration of positively charged pyridinium moiety, attracted by the negatively charged interior of the transmembrane potential of mitochondria. To the best of our knowledge, the presented AIEgens hold the lowest working concentration comparing with other previously reported AIEgens for mitochondria-specific imaging.[39,43,44] Considering the great significance of photostability for evaluating a fluorescence imaging agent, continuous excitation and sequential scanning of AIEgen-stained HeLa cells with confocal microscope were carried out. As depicted in Figure 2I–M, in the case of MitoTracker Green, a large drop of fluorescence intensity to 38% of its initial value was observed during 40 scans with total irradiation time of 15 min. By contrast, the fluorescence intensities of both TTPy and MeTTPy remain almost constant under the same conditions, revealing the unique advantage of AIEgens in term of photostability.

It has been reported that cancer cells generally have a higher level of lactate secretion than normal cells, which is caused by the elevated glycolysis of cancer cells, meanwhile,

the positive ions on the cancer cell surfaces can be removed by the excessively secreted lactate anions, resulting in negatively charged surface.[40] Moreover, higher mitochondrial membrane potential (MMP) of cancer cells than normal cells with a difference of at least 60 mV, which could lead to significantly higher mitochondrial upconcentration of lipophilic cations, has been proven to be a powerful protocol for discriminating cancer cells over normal cells.[39,45] Inspiringly, it was speculated that the presented AIEgens inherently having both positive charge and mitochondrial-targeting capability would be promising candidates for the differentiation of the cancer cells from normal cells. To verify these hypotheses, various cancer cells and normal cells were incubated with 200×10^{-9} M of AIEgens within 20 min. Taking MeTTPy as an example, observation by confocal imaging suggests the AIEgens were efficiently accumulated and "light up" the mitochondria of all the investigated cancer cells including DLD1, KM12, HeLa, A431, and HCT116 cells, with a very high signal-to-noise ratio (**Figure 3**). On the contrary, the normal-cells-staining experiments involving HLF, NCM460, and LX2 cells provided much weaker fluorescence intensity and contrast than that of cancer cells. These results consequently demonstrated that the developed FR/NIR AIEgens were able to serve as extraordinary bioimaging agents for selectively staining cancer cells. This system requires neither extra cancer cell-specific targeting ligand with high cost nor complicated preparation, thus allowing the potential applications in the area of early-stage cancer diagnosis and precise cancer treatment. In order to further investigate the targeted mechanism, both the analysis of MMP difference and inhibitor block experiment have been done. First, the analysis of MMP difference was conducted by using a MMP-dependent molecule, JC-1, as the indicator. JC-1 emits green fluorescence in its monomer form at low MMP, while it aggregates at high MMP and emits red light. Based on this property, MMP of cells can be determined by the ratio between red and green fluorescence intensities. As shown in Table S2 and Figure S7 (Supporting Information), normal cells provided lower Red/Green ratio than all involved cancer cells, indicating the lower MMP of normal cells. These data are in good accordance with the results of differentiation of cancer cells from normal cells by the presented AIEgens, suggesting that MMP difference is an important parameter for these two AIEgens to selectively target with cancer cells. Second, inhibitor block experiment was carried out by employing carbonyl cyanide *m*-chlorophenyl hydrazone (CCCP) as inhibitor to decrease MMP of cells. Taking HeLa cells as an example, they were pretreated with CCCP followed by staining with MitoTracker Green or MeTTPy, and it was observed that the fluorescence intensity of mitochondria-specific cell imaging is much lower comparing with that without pretreatment (Figure S8, Supporting Information). This result can be attributed to the decreased electrostatic attraction between dyes and HeLa cells upon CCCP treatment. It seems reasonable to infer that MMP difference is the driving force for realizing the specific staining of cancer cells over normal cells. Moreover, it is believed that the higher mitochondria density of cancer cells could also contribute to the promoted accumulation of these AIEgen in cancer cells (Table S3 and Figure S9, Supporting Information).

Mitochondria that relate with many considerably important biofunctions including energy production and cellular signaling have been recognized to be vital subcellular organelles to eukaryotic cells, and it has been realized that PDT-induced cell apoptosis is mainly caused by the damage of mitochondria.[46] Therefore, mitochondria represent an ideal targeting site for PDT study. Encouraged by the attractive properties of these AIEgens in both mitochondria-specific targeting and selective accumulation toward cancer cells. TTPy and MeTTPy were employed as PSs for PDT application. The preliminary experiment was conducted by evaluating the efficiency of ROS generation, which undoubtedly plays a critical role in PDT. The strong absorptions of both TTPy and MeTTPy in the visible light region supported the utilization of easy-to-reach and less harmful white light as irradiation source. Two strategies involving 2′,7′-dichlorodihydrofluorescein diacetate (H2DCF-DA) and 9,10-anthracenediyl-bis(methylene) dimalonic acid (ABDA) as indicators were, respectively, performed. As illustrated in **Figure 4**A, H2DCF-DA alone was almost non-emissive, while its emission intensity was triggered and rapidly raised with increasing irradiation time in the presence of TTPy and MeTTPy, reaching 19- and 21-fold enhancement in 65 s, thus suggesting the high-efficiency ROS generation of TTPy and MeTTPy. As a commercially available ROS probe, ABDA

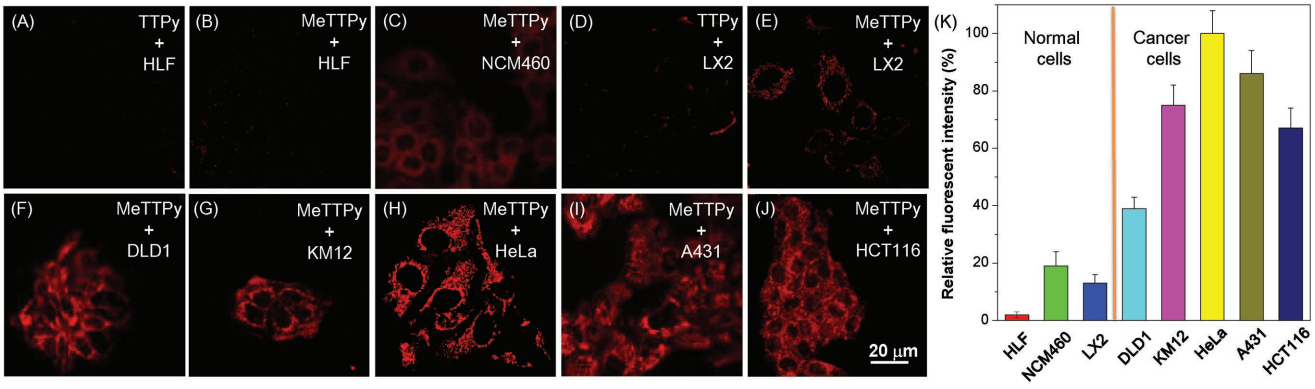

Figure 3. Differentiation of cancer cells from normal cells by AIEgens. A–J) Fluorescence images of different normal cells (A–E) and cancer cells (F–J) stained with TTPy or MeTTPy (200×10^{-9} M) for 20 min. K) Relative fluoresence intensity of different cells incubated with MeTTPy (200×10^{-9} M) for 20 min, the intensity data were measured by MATLAB R2015. Scale bar = 20 μm.

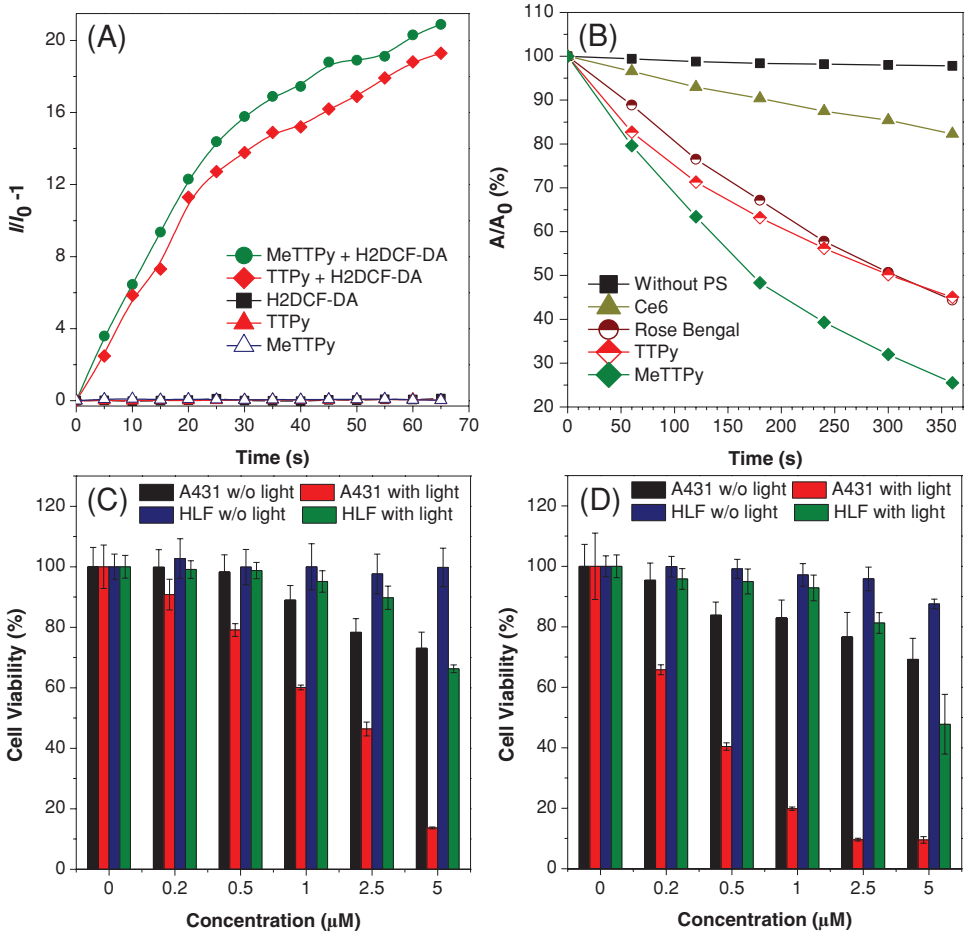

Figure 4. A,B) ROS generation and C,D) selective killing of cancer cells through PDT. A) ROS generation upon white light irradiation using H2DCF-DA as indicator. B) Decomposition rates of ABDA in the presence of different PSs under light irradiation, where A_0 and A are the absorbance of ABDA at 378 nm. C,D) Cell viability of A431 cancer cells and HLF normal cells stained with different concentrations of TTPy (C) and MeTTPy (D) in the absence or presence of white light irradiation.

that can be decomposed by ROS showing the changes of its absorbance, was further used to compare the ROS-producing capability of the presented AIEgens with other well-known PSs having high efficiencies. As depicted in Figure 4B and Figure S10 (Supporting Information), after 6 min exposure to white light, 55 and 74.5% of ABDA were consumed in the presence of TTPy and MeTTPy, respectively, while the absorbance of ABDA remained almost constant without PS. Commercially available Ce6 and Rose Bengal, which are the most widely used and reputable PSs for PDT, were investigated under the same conditions. It was observed that 16.7 and 55.6% of ABDA were decomposed by them, respectively, demonstrating that in terms of ROS generation, the performance of both TTPy and MeTTPy are far superior to Ce6; TTPy is comparative with Rose Bengal; excitedly, MeTTPy is much better than Rose Bengal. In addition, 71.91 and 90.7% of ROS quantum yields for TTPy and MeTTPy were determined using ABDA as indicator, and Rose Bengal as the standard photosensitizer (Figure S11, Supporting Information). To the best of our knowledge, MeTTPy would be the best in terms of ROS generation comparing with various previously reported PSs. It was believed that the highly efficient ROS generation of both TTPy and MeTTPy are benefited from their small singlet–triplet energy gaps (0.565 eV for TTPy, 0.541 eV for MeTTPy), which facilitate the ISC process from S1 to T1 and considerably improve the yield of the triplet excited state. While comparing with TTPy, the more efficient ROS production of MeTTPy can be ascribed to its smaller singlet–triplet energy gap resulting from the stronger D–A effect.

The presented AIEgens were further utilized as PSs for PDT application by quantitatively evaluating on A431 cancer cells through standard 3-(4,5-dimethylthiazol-2-yl)-2,5-diphenyltetrazolium bromide (MTT) assay. The study of dose-dependent cytotoxicity revealed that both TTPy and MeTTPy exhibited relatively low cytotoxicity in dark condition, suggesting their acceptable biocompatibility. Upon white light irradiation, cell viability was gradually and rapidly decreased, as illustrated in Figure 4C,D, 36% of cell viability remained in the presence of 2.5×10^{-6} M of TTPy, and 2.5×10^{-6} M of MeTTPy can cause almost complete cell death with only 8% of cell viability remained. These results demonstrated that both TTPy and MeTTPy were considerably powerful for cancer cell ablation through PDT pathway, and MeTTPy displayed better therapeutic output than TTPy, which is in good accordance with experimental data of ROS generation. Furthermore, to investigate the selectivity of

AIEgens in killing cancer cells over normal cells, experiments of dose-dependent cytotoxicity were conducted by using HLF normal cells as a model. No obvious drop of the viability of HLF cells was observed in both the absence and presence of white light illumination, indicating the negligible damage toward normal cells benefiting from both inefficient accumulation of these AIEgens in normal cells and high ROS-resistant ability of normal cells (Figure S12, Supporting Information). The excellent ability of these AIEgens in specific cancer cells imaging and killing make them promising in cancer theranostics.

Inspired by its outstanding performance in cellular experiments, MeTTPy was chosen as PS for in vivo PDT application involving A431-skin-tumor-bearing nude mice. As depicted in **Figure 5**A and Figure S13 (Supporting Information), after intratumoral injection of MeTTPy (4×10^{-3} M, 100 µL/200 mm^3 tumor) for 5 min, intense fluorescence signals were captured at the tumor site, which was continuously imaged for the duration from 5 min to 24 h. At 24 h postinjection, tumor fluorescence was still significantly observed, suggesting the remarkable tumor retention property of MeTTPy. To image the fluorescence of the tumor and other organs, the mice were sacrificed at 24 h postinjection of MeTTPy, and ex vivo fluorescence images of isolated tissues are shown in Figure 5B and Figure S14 (Supporting Information). It was found that the AIEgen effectively accumulated in the tumor tissue yielding high emission intensity, meanwhile, no or very low level of fluorescence signals originating from major organs (including spleen, liver, intestine, kidney, lung, and heart) was determined, evidently confirming the excellent specificity of MeTTPy for tumor imaging. In the following study, the dose-dependent in vivo imaging experiments involving different concentrations (0.16, 0.8, 4, and 20×10^{-3} M) of MeTTPy have been carried out. As depicted in Figure S15 (Supporting Information), after intratumoral injection of MeTTPy solution (100 µL/200 mm^3 tumor) with different concentrations, fluorescence signals were captured at the tumor site. At each investigated time point including 10 s, 30 s, 1 min, 5 min, 30 min, 1 h, and 2 h, the fluorescence intensity of tumor was gradually enhanced with increasing concentration of MeTTPy. For instance, at 2 h postinjection, tumor fluorescence was enhanced fivefold significantly through increasing the concentration of MeTTPy from 0.16 to 20×10^{-3} M, suggesting a "turn-on" imaging effect of AIEgen. To assess the in vivo behaviors of MeTTPy, pharmacokinetics study was performed. In the blood-circulation experiment, a circulating half-life of 2.75 h in blood stream was obtained (Figure S16, Supporting Information). In the primary study on therapeutic effect of MeTTPy, mice-bearing A431 tumor were treated with intratumoral injections of PBS, DMSO, or MeTTPy (4×10^{-3} M, 100 µL/200 mm^3 tumor). 30 min after injection, the tumor sites of the mice were exposed to white light at a power density of 18 mW cm^{-2} for 10 min, and the mice that are injected with the same dose of MeTTPy but without light illumination was employed as the control. The results showed that comparing with control groups, the tumor growth of mice with both the injection of MeTTPy and light irradiation was obviously hindered (Figures S17A,B, Supporting Information), indicating the good efficacy of MeTTPy in PDT even with ultralow irradiation power. In order to further clarify the tumor inhibition performance of MeTTPy, the mice in different groups were sacrificed on day 14, and the proliferative activity of tumors was evaluated by inmmunohistochemical staining of paraffin specimens of A431 tumors using the proliferative marker Ki67. A significant decrease in Ki67-positive cell proportion from 32.2 to 5.3% was documented in A431 tumors treated with MeTTPy and light irradiation (Figure S17C,D,

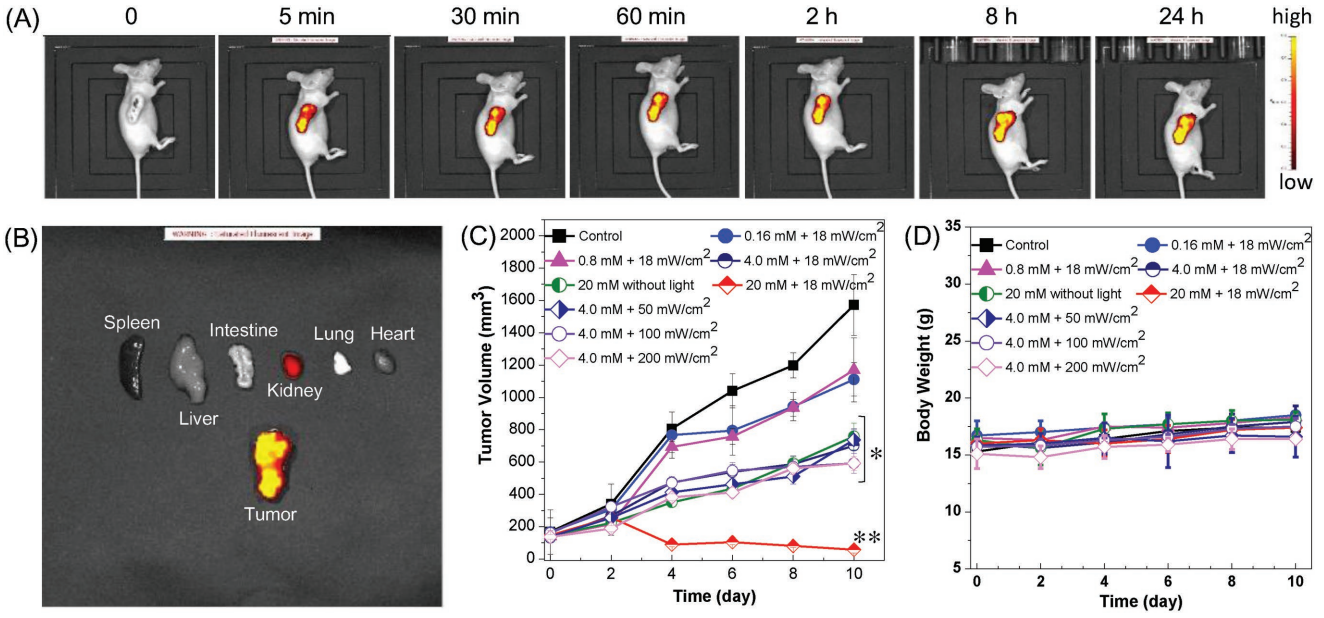

Figure 5. In vivo imaging and PDT application. A) Biodistribution of MeTTPy in A431-tumor-bearing mice after intratumoral injection of MeTTPy (4×10^{-3} M, 100 µL/200 mm^3 tumor) at different time. B) Ex vivo fluorescence imaging of various organs and tumor tissue from mice injected with MeTTPy. The mice were sacrificed at 24 h postinjection. C) The volume growth curves of tumors at different time points post-treatment in different groups ($n = 3$, $^*P < 0.05$ comparing with control group, $^{**}P < 0.01$ comparing with control group, data represent mean ± SD). D) Body weight measurement of the mice in each group. The data represent the mean ± SD.

Supporting Information), strongly suggesting that MeTTPy can inhibit cancer cell proliferation by the way of PDT. It was noted that in the absence of white light treatment, MeTTPy can slightly slow down the growth of tumor, which could be resulted from chemotherapeutic effect of MeTTPy or unavoidable light illumination during mice cultivation after intratumoral injection of MeTTPy. In addition, in order to study whether MeTTPy cause in vivo side toxicity, major organs of sacrificed mice in each treatment group were also excised and sectioned for histological hematoxylin and eosin (H&E) staining. As shown in Figure S18 (Supporting Information), no noticeable tissue damage and inflammatory lesion can be observed in the heart, liver, spleen, lung, kidney, and intestine organs from all the treatment groups of mice, demonstrating the harmlessness of MeTTPy toward major organs. The dose-dependent in vivo therapy study was further performed with intratumoral injection of MeTTPy solutions with different concentrations (0.16, 0.8, 4, and 20×10^{-3} M) by using white light at a power density of 18 mW cm^{-2}. As shown in Figure 5C, Figures S19 and S20 (Supporting Information), the inhibitory effect of tumor growth was dramatically promoted with raising concentrations of MeTTPy solutions from 0.16 to 20×10^{-3} M. When MeTTPy with the concentration of 20×10^{-3} M was utilized, tumor can be almost completely eliminated after 10 d, indicating its extremely high efficiency in PDT application. Considering that the previously reported photosensitizers usually only hindered the tumor growth, but not directly reduced the tumor size, MeTTPy would be excellent candidate for PDT in clinic. In order to comprehensively evaluate the developed photosensitizers, power density-dependent therapeutic study was then carried out by using 4×10^{-3} M of MeTTPy upon white light illumination with different power densities including 18, 50, 100, and 200 mW cm^{-2}. It was found that only slight enhancement of therapeutic effect was observed with the increase of the light power from 18 to 200 mW cm^{-2} (Figure 5C), suggesting that white light with ultralow power as 18 mW cm^{-2} is sufficient to efficiently arouse the ROS generation. Noteworthy, the negligible side toxic effect of the treatment of "MeTTPy + light" was also clearly verified by the negligible body weight losses of mice as compared to those of control groups (Figure 5D and Figure S17E, Supporting Information).

In summary, we have developed a simple protocol to prepare a novel type of theranostic agents (TTPy and MeTTPy) possessing typical AIE characteristics and intense FR/NIR emission. This presented theranostic system is able to selectively stain cancer cells over normal cells with high specificity, without the need for any extra targeting ligands. Noteworthy, the ROS generation efficiency of MeTTPy is extraordinarily high with up to 90.7% of ROS quantum yield, even far superior to both Ce6 and Rose Bengal, which are two of the most efficient and popularly used PSs. The high-performance ROS generation could be attributed to the efficient ISC process from S1 to T1 benefiting from both high D–A strength and the existence of heteroatoms. Thanks to the long emission wavelength, excellent photostability, good biocompatibility, high specificity of targeting cancer cells, and effective ROS production, both in vitro and in vivo results revealed that these AIEgens are promising alternatives for cancer theranostics involving the modality of image-guided PDT. This successful example of AIE theranostics design will provide a blueprint for the next generation of theranostic anticancer therapeutics, and stimulate the development of simple and efficient theranostic agents for potential clinical applications.

Supporting Information

Supporting Information is available from the Wiley Online Library or from the author.

Acknowledgements

This work was partially supported by the National Basic Research Program of China (973 Program; 2013CB834701 and 2013CB834702), the University Grants Committee of Hong Kong (AoE/P-03/08), the Research Grants Council of Hong Kong (16301614, 16305015, and N_HKUST604/14), Innovation and Technology Commission (ITC-CNERC14SC01), the National Science Foundation of China (81372274, 81501591, and 8141101080), the Science and Technology Planning Project of Guangdong Province (2014A030313033 and 2014A050503037), and the Shenzhen Science and Technology Program (Grant Nos. JCYJ20130402103240486 and JCYJ20160509170535223). B.Z.T. is also grateful for the support from the Guangdong Innovative Research Team Program of China (201101C0105067115). Animal experiments were approved by the China Committee for Research and Animals Ethics in compliance with the law on experimental animals.

Conflict of Interest

The authors declare no conflict of interest.

Keywords

aggregation-induced emission, FR/NIR emission, molecular design, photodynamic therapy, theranostic materials

Received: April 2, 2018
Revised: July 10, 2018
Published online:

[1] J.-M. Idée, S. Louguet, S. Ballet, C. Corot, *Quant. Imaging Med. Surg.* **2013**, *3*, 292.
[2] K. Rajesh, S. S. Weon, S. Kyoung, W. Y. Kim, S. Koo, S. Bhuniya, J. S. Kim, *Chem. Soc. Rev.* **2015**, *44*, 6670.
[3] J. Xie, S. Lee, X. Chen, *Adv. Drug Delivery Rev.* **2010**, *62*, 1064.
[4] M. S. Muthu, D. T. Leong, L. Mei, S. S. Feng, *Theranostics* **2014**, *4*, 660.
[5] T. Lammers, S. Aime, W. E. Hennink, G. Storm, F. Kiessling, *Acc. Chem. Res.* **2011**, *44*, 1029.
[6] X. Li, J. Kim, J. Yoon, X. Chen, *Adv. Mater.* **2017**, *29*, 1606857.
[7] M. Gao, F. Yu, C. Lv, J. Choo, L. Chen, *Chem. Soc. Rev.* **2017**, *46*, 2237.
[8] Y. Yu, B. Y. L. Mok, X. J. Loh, Y. N. Tan, *Adv. Healthcare Mater.* **2016**, *5*, 1844.
[9] Z. Yang, J. H. Lee, H. M. Jeon, J. H. Han, N. Park, Y. He, H. Lee, F. S. Hong, C. Kang, J. S. Kim, *J. Am. Chem. Soc.* **2013**, *135*, 11657.
[10] B. N. G. Giepmans, S. R. Adams, M. H. Ellisman, R. Y. Tsien, *Science* **2006**, *312*, 217.
[11] T. Terai, T. Nagano, *Curr. Opin. Chem. Biol.* **2008**, *12*, 515.

[12] P. Agostinis, K. Berg, K. A. Cengel, T. H. Foster, A. W. Girotti, S. O. Gollnick, S. M. Hahn, M. R. Hamblin, A. Juzeniene, D. Kessel, M. Korbelik, J. Moan, P. Mroz, D. Nowis, J. Piette, B. C. Wilson, J. Golab, *CA-Cancer J. Clin.* **2011**, *61*, 250.
[13] J. P. Celli, B. Q. Spring, I. Rizvi, C. L. Evans, K. S. Samkoe, S. Verma, B. W. Pogue, T. Hasan, *Chem. Rev.* **2010**, *110*, 2795.
[14] M. Ethirajan, Y. Chen, P. Joshi, R. K. Pandey, *Chem. Soc. Rev.* **2011**, *40*, 340.
[15] D. E. Dolmans, D. Fukumura, R. K. Jain, *Nat. Rev. Cancer* **2003**, *3*, 380.
[16] A. P. Castano, P. Mroz, M. R. Hamblin, *Nat. Rev. Cancer* **2006**, *6*, 535.
[17] L. Cheng, C. Wang, L. Z. Feng, K. Yang, Z. Liu, *Chem. Rev.* **2014**, *114*, 10869.
[18] J. Wang, L. Zhang, M. Chen, S. Gao, L. Zhu, *ACS Appl. Mater. Interfaces* **2015**, *7*, 23248.
[19] J. Tian, L. Ding, H. J. Xu, Z. Shen, H. Ju, L. Jia, L. Bao, S. Yu, *J. Am. Chem. Soc.* **2013**, *135*, 18850.
[20] J. Tian, L. Ding, H. Ju, Y. Yang, X. Li, Z. Shen, Z. Zhu, J. S. Yu, C. J. Yang, *Angew. Chem., Int. Ed.* **2014**, *53*, 9544.
[21] J. Ge, M. Lan, B. Zhou, W. Liu, L. Guo, H. Wang, Q. Jia, G. Niu, X. Huang, H. Zhou, X. Meng, P. Wang, C. S. Lee, W. Zhang, X. Han, *Nat. Commun.* **2014**, *5*, 4596.
[22] W. Wu, D. Mao, F. Hu, S. Xu, C. Chen, C.-J. Zhang, X. Cheng, Y. Yuan, D. Ding, D. Kong, B. Liu, *Adv. Mater.* **2017**, *29*, 1700548.
[23] J. Luo, Z. Xie, J. W. Y. Lam, L. Cheng, H. Chen, C. Qiu, H. S. Kwok, X. Zhan, Y. Liu, D. Zhu, B. Z. Tang, *Chem. Commun.* **2001**, 1740.
[24] J. Mei, Y. Hong, J. W. Y. Lam, A. Qin, Y. Tang, B. Z. Tang, *Adv. Mater.* **2014**, *26*, 5429.
[25] J. Mei, N. L. C. Leung, R. T. K. Kwok, J. W. Y. Lam, B. Z. Tang, *Chem. Rev.* **2015**, *115*, 11718.
[26] R. T. K. Kwok, C. W. T. Leung, J. W. Y. Lam, B. Z. Tang, *Chem. Soc. Rev.* **2015**, *44*, 4228.
[27] Y. Hong, J. W. Y. Lam, B. Z. Tang, *Chem. Soc. Rev.* **2011**, *40*, 5361.
[28] H. Shi, J. Liu, J. Geng, B. Z. Tang, B. Liu, *J. Am. Chem. Soc.* **2012**, *134*, 9569.
[29] S. Xu, Y. Yuan, X. Cai, C.-J. Zhang, F. Hu, J. Liang, G. Zhang, D. Zhang, B. Liu, *Chem. Sci.* **2015**, *6*, 5824.
[30] L. Yang, X. Wang, G. Zhang, X. Chen, G. Zhang, J. Jiang, *Nanoscale* **2016**, *8*, 17422.
[31] D. Wang, H. Su, R. T. K. Kwok, G. Shan, A. C. S. Leung, M. M. S. Lee, H. H. Y. Sung, I. D. Williams, J. W. Y. Lam, B. Z. Tang, *Adv. Funct. Mater.* **2017**, *27*, 1704039.
[32] K. Han, S.-B. Wang, Q. Lei, J.-Y. Zhu, X.-Z. Zhang, *ACS Nano* **2015**, *9*, 10268.
[33] H. S. Choi, S. L. Gibbs, J. H. Lee, S. H. Kim, Y. Ashitate, F. B. Liu, H. Hyun, G. Park, Y. Xie, S. Bae, M. Henary, J. V. Frangioni, *Nat. Biotechnol.* **2013**, *31*, 148.
[34] A. L. Antaris, H. Chen, K. Cheng, Y. Sun, G. Hong, C. Qu, S. Diao, Z. Deng, X. Hu, B. Zhang, X. Zhang, O. K. Yaghi, Z. R. Alamparambil, X. Hong, Z. Cheng, H. Dai, *Nat. Mater.* **2016**, *15*, 235.
[35] T. Yogo, Y. Urano, Y. Ishitsuka, F. Maniwa, T. Nagano, *J. Am. Chem. Soc.* **2005**, *127*, 12162.
[36] S. O. McDonnell, M. J. Hall, L. T. Allen, A. Byrne, W. M. Gallagher, D. F. O'Shea, *J. Am. Chem. Soc.* **2005**, *127*, 16360.
[37] W. Zhao, Z. He, J. W. Y. Lam, Q. Peng, H. Ma, Z. Shuai, G. Bai, J. Hao, B. Z. Tang, *Chem* **2016**, *1*, 592.
[38] Y. Yuan, R. T. K. Kwok, B. Z. Tang, B. Liu, *J. Am. Chem. Soc.* **2014**, *136*, 2546.
[39] C. Gui, E. Zhao, R. T. K. Kwok, A. C. S. Leung, J. W. Y. Lam, M. Jiang, H. Deng, Y. Cai, W. Zhang, H. Su, B. Z. Tang, *Chem. Sci.* **2017**, *8*, 1822.
[40] B. Chen, W. Le, Y. Wang, Z. Li, D. Wang, L. Ren, L. Lin, S. Cui, J. J. Hu, Y. Hu, P. Yang, R. C. Ewing, D. Shi, Z. Cui, *Theranostics* **2016**, *6*, 1887.
[41] Z. R. Grabowski, K. Rotkiewicz, *Chem. Rev.* **2003**, *103*, 3899.
[42] S. Aoki, D. Kagata, M. Shiro, K. Takeda, E. Kimura, *J. Am. Chem. Soc.* **2004**, *126*, 13377.
[43] E. Zhao, H. Deng, S. Chen, Y. Hong, C. Y. T. Leung, J. W. Y. Lam, B. Z. Tang, *Chem. Commun.* **2014**, *50*, 14451.
[44] C. W. T. Leung, Y. Hong, S. Chen, E. Zhao, J. W. Y. Lam, B. Z. Tang, *J. Am. Chem. Soc.* **2013**, *135*, 62.
[45] B. C. Lan, *Annu. Rev. Cell Biol.* **1988**, *4*, 155.
[46] J. S. Modica-Napolitano, J. R. Aprille, *Adv. Drug Delivery Rev.* **2001**, *49*, 63.